COMPOSITION AND FREQUENCY OF IMPACT RESIDUES DETECTED ON LDEF SURFACES

R. P. Bernhard*, F. Hörz**, M. E. Zolensky**
T. H. See*, R. A. Barrett*
*C23, Lockheed ESC, Houston, TX 77058
**SN4, NASA JSC, Houston, TX 77058

ABSTRACT

A total of 1225 craters (10 to 4000 μm in diameter) detected on gold and aluminum surfaces on LDEF have been examined by means of SEM/EDX analysis to determine the compositional make-up of the projectile residues (*i.e.*, natural versus man-made debris). Of these, 517 craters contain insufficient residue to permit identification, 382 craters were made by natural cosmic dust, and 113 impacts resulted from man-made debris. However, the majority of craters analyzed were in aluminum targets and it is not possible to detect aluminum projectiles under these conditions; therefore, man-made particles may be underestimated. For the gold surfaces the ratio of natural to man-made impactors is ~2:1, with ~85% of all man-made craters resulting from impacts by aluminum (metallic or oxidized). The presence of a substantial population of man-made impactors on LDEF's trailing edge was unexpected and required modifications of existing orbital-debris models.

1. INTRODUCTION

The Long Duration Exposure Facility (LDEF) was placed in low-Earth orbit (LEO) in 1984, and recovered 5.7 years later. It was host to several experiments specifically designed to characterize the meteoroid and orbital-debris environment in LEO. LDEF affords unique opportunities because it was (1) a gravity-stabilized, non-spinning platform that permits characterization of particle fluxes as a function of specific viewing direction relative to the platform's direction of orbital motion; all other surfaces retrieved from space were from spin-stabilized spacecraft; and (2) the unexpectedly long mission duration (5.7 years) combined with large instrument surfaces provides time-area products that are orders of magnitude larger than previous opportunities. Analysis of LDEF surfaces may be viewed as a unique opportunity to characterize the hypervelocity particle environment in LEO for impactors <1 mm in diameter.

One experiment dedicated to hypervelocity particle studies was the "Chemistry of Micrometeoroids Experiment" (CME) that exposed two substantially different instruments, one active, the other passive (Ref. 1). The active instrument consisted of clamshell-type devices that opened and closed in order to minimize contamination that could result from ground handling of the payload, or during LDEF's deployment and retrieval. When open, this instrument exposed ~0.82 m^2 of high-purity gold substrate, ~0.5 mm thick, on LDEF's trailing edge relative to LDEF's direction of motion (*i.e.*, in LDEF Bay A03). This location and viewing direction inherently yields the smallest particle flux on a non-spinning platform (Ref. 2); this instrument cycled between the open and closed positions for an effective exposure time for the gold collectors of only 3.4 years (Ref. 1). For these reasons the Au collectors exhibited relatively low crater densities.

In contrast, the passive instrument continuously exposed ~1.1 m^2 of aluminum (series 1100-T4, annealed; >99% Al) for the entire 5.7 years. It was located in Bay A11, which pointed some 52° off LDEF's forward-facing direction (*i.e.*, leading edge), for which relatively high particle fluxes were predicted (Ref. 2) and indeed found (Ref. 1). The instrument consisted of six individual aluminum panels (~41 x 46 cm, each) ~3.2 mm thick; four of which have been analyzed to date, although only three were included in this report.

Clearly, micrometeoroid and debris particles impinged on all sides of the LDEF spacecraft, and numerous surfaces exist that can complement the dedicated instruments. Of special interest are uniform materials, preferably of known cratering behavior, that were exposed in all LDEF pointing directions. Only two surfaces satisfied these criteria: (a) The experiment-tray clamps and (b) LDEF's structural frame.

All 86 experiment trays on LDEF were held in place by a series of chromic-anodized aluminum (6061-T6) clamps (Figure 1); eight clamps were used to attach the experiment trays on each of the 12 sides of LDEF, while trays on the Earth and space ends were held in place by 12 clamps each. Each clamp was fastened to the spacecraft frame using three stainless-steel hex-head bolts. Individual clamps measured ~4.8 cm x 12.7 cm x 0.45 cm which resulted in an average surface area of ~58 cm^2 each, minus the area covered by the bolts. All 774 clamps were surveyed for craters >0.5 mm in diameter during LDEF deintegration at the Kennedy Space Center. Subsequent scanning of selected clamps for smaller impact features has been carried out at the Johnson Space Center.

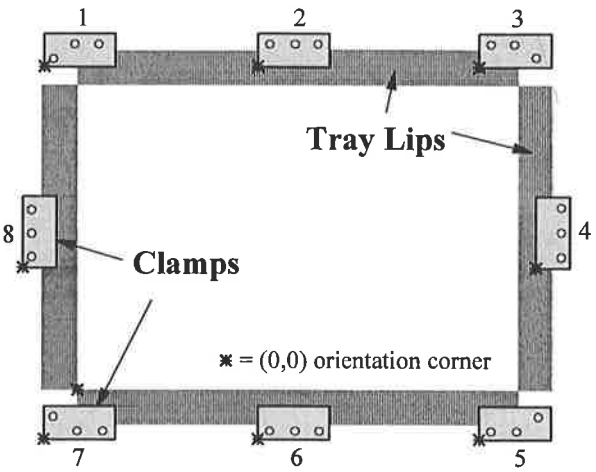

Figure 1. Diagram illustrating the position and associated number of the tray clamps for a peripheral tray (Rows 1-12) on LDEF.

The present compositional studies focus on the variability of hypervelocity particles in LEO, such as man-made versus natural particles, on their relative and absolute frequencies, and on potential implications regarding their sources. Currently, we have performed Scanning Electron Microscopy (SEM) and Energy Dispersive X-ray (EDX) analyses on 199 craters >30 μm in diameter from the Au-collectors, 611 craters >40 μm in diameter from three of the six A11 aluminum panels, and 202 craters from 44 clamps, for a total 1012 impacts.

Detectable residues were classified as either natural or man-made materials, with each of these two main populations being further subdivided into subclasses. Of the residues categorized as natural, chondritic-type compositions dominated, while monomineralic, mafic-silicate compositions and Fe-Ni-S particles were found to a lesser degree. Man-made debris compositions include aluminum (only detectable on the gold collectors), spacecraft thermal paint, electrical components, and spacecraft structural hardware.

2. ANALYTICAL PROCEDURES

Projectile compositions were determined using an ISI-SR50 SEM, and a LINK eXL EDX analyzer using a Si(Li) detector, arranged at 90° to the beam path. In general, we followed the analytical procedures and compositional particle classifications developed during the analysis of interplanetary dust recovered from the stratosphere (Refs. 3, 4), and from space-retrieved surfaces such as the Solar Maximum or Palapa satellites (Refs. 5, 6, 7). Although we characterize our analyses as qualitative and of a survey-type nature, considerable effort was spent in optimizing the signal to noise ratio of the X-ray spectra. Initially it was found that an uncomfortably large fraction of craters yielded spectra that contained no detectable signal above that of the background. Therefore, we used a number of craters to investigate a range of electron-beam geometries (diameter and take-off angle), low- and high-beam voltages, and widely variable count times (minutes to hours) in search of the optimum instrument settings. From these efforts it was determined that a relatively high-beam voltage (25-20 KeV), long count times (500-1000 seconds), with the specimen tilted at 30° yielded the best results. High-beam voltages are believe best because the surface relief of the crater interiors tends to be uneven permitting excitation of more near-surface specimen volume compared to less penetrative, low-energy electrons. Count times in excess of 1000 seconds did not appreciably improve the signal to noise ratios and, therefore, did not warrant the additional expenditure of resources.

In general, surface contamination was not a significant problem because the composition of such contamination tended to differ dramatically from that of the projectile residues. Nevertheless, we observed Si-Ca rich deposits, presumably outgassed RTV (Ref. 12), in some crater interiors. Interestingly, such deposits can have distinctly asymmetric distributions within some craters, substantiating the macroscopic LDEF observations of highly directional flow of gaseous contaminants and their condensates. We also observed some intrinsic, heterogeneously distributed contaminants (*i.e.*, As in the gold and Si in the aluminum) that were the result of manufacturing processes and procedures used in the production of the CME collectors. The anodized layer on the aluminum surfaces varied from plate to plate and clamp to clamp, but background from this source was taken into consideration.

Within the craters investigated in this study the projectile residues typically occur as discontinuous melts lining the bottom, walls and/or rims of the craters. The thickness of these linings is typically much less than the depth of penetration (2-3 μm) of the electron beam. Therefore, the volume from which X-rays are being excited is invariably a mixture of the collector and projectile compositions, and is why most spectra reflect the major elements present in both the target and projectile materials. However, some melt or vapor deposits may become so thin that they are beyond the detection threshold. As a result, projectile composition may not be obtained from some craters using SEM/EDX techniques, especially those craters in aluminum surfaces which resulted from impacts by aluminum particles. On the other hand, Au is in very low concentration in man-made and natural impactors; thus, the high-purity gold collectors (>99.99% Au) -- by design -- will yield favorable signal to noise ratios for *all* particles.

3. PARTICLE CLASSIFICATION

Our particle classification fully adopts the criteria accepted in the classification of interplanetary dust recovered from the stratosphere (Ref. 3, 4), and of man-made debris found on Solar Max and Palapa surfaces (Ref. 5, 6, 7). Consistent with the latter, the LDEF residues could be classified into three main categories, natural, man-made and indeterminate. As detailed below, specific subgroups may be established within these major classes.

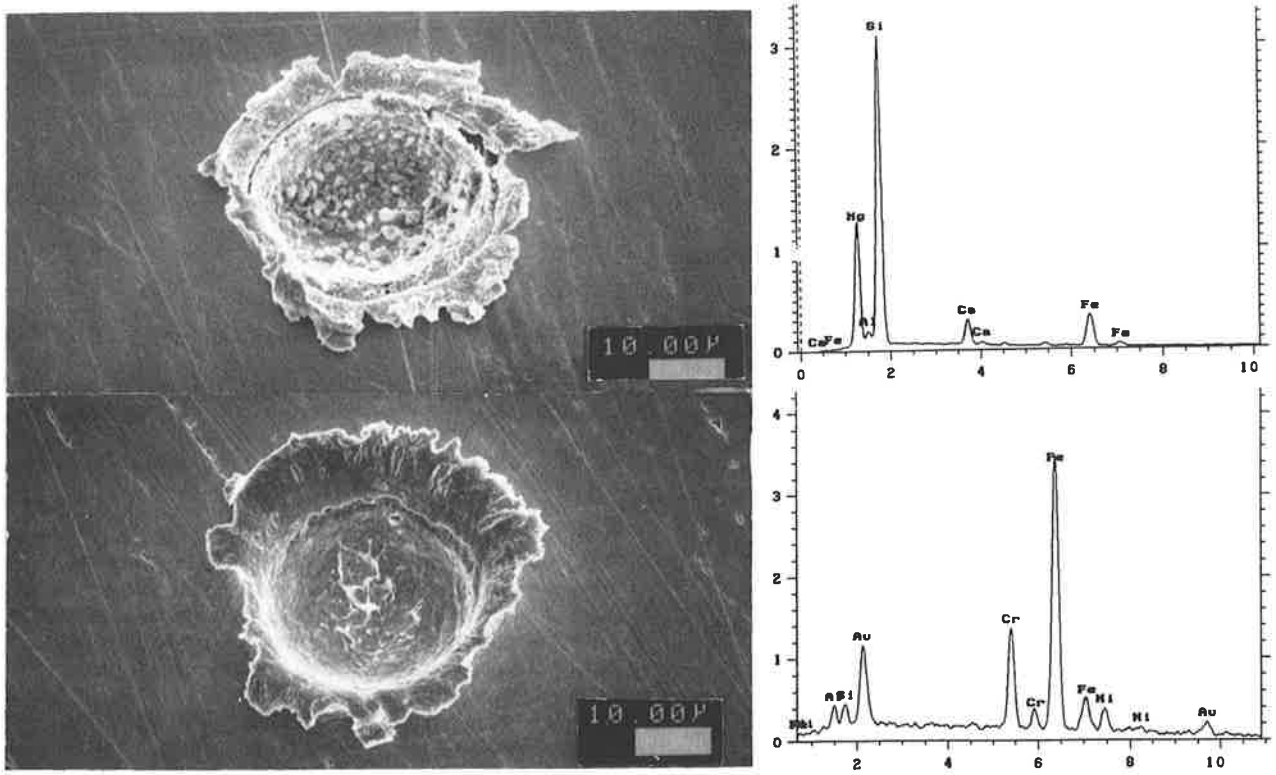

Figure 2. Scanning electron micrographs and Energy Dispersive X-ray spectra representing micrometeoritic (chondritic) and man-made orbital debris (stainless steel) residues present in impact features detected on exposed LDEF surfaces.

While signal to noise ratios may vary strongly from crater to crater, it is possible to assign most residues to one of the three major categories with relative ease and confidence; nevertheless, judgment calls are necessary on occasion, albeit rarely. However, one can obtain substantially different spectra from various locations within individual craters, especially for those craters that possess mixtures of molten material and unmelted fragments. The latter yield spectra consistent with component minerals of dust grains (*e.g.*, olivines or pyroxenes) that differ distinctly from the melted bulk residue, yet the bulk compositions were used exclusively for particle classification purposes. Variability within the pure melts was observed as well, with the largest variations occurring in those craters that contained unmelted residues, suggesting the presence of incompletely mixed mineral melts (Refs. 13, 14). Generally, this melt variability relates to subtly different elemental ratios among different spectra obtained from the same specimen. Nevertheless, this specimen heterogeneity does not affect the major classifications into natural and man-made particle sources (Figure 2).

3.1 Natural Particles

The natural particles were divided into three subclasses (1) chondritic, (2) monomineralic silicates, and (3) Fe-Ni sulfides. Chondritic particles generally contained little, if any, clastic materials, but largely consisted of a relatively well-mixed and homogenized, fine-grain matrix. The monomineralic silicates were characterized by high concentrations of Si, Mg, and Fe, and were found in molten form and/or as unmelted fragments of olivine and pyroxene (Figure 2). The Fe-Ni sulfide type particles were generally found as melt residues, typically in association with minor quantities of chondritic melt.

A detailed structural and compositional analysis of several impactor residues was performed utilizing transmission electron microscopy (TEM), energy dispersive spectroscopy, and electron diffraction (*e.g.*, Ref. 4). Such studies aim at detailed characterization of unmolten projectile residues, rather than melts. The structural state and detailed phase chemistry of individual minerals reflects on their condition(s) of formation (*e.g.*, on early solar system processes in the case of interplanetary dust; Ref. 4). Such studies are just beginning for LDEF specimen.

For these purposes, part of the residues were removed from several craters with a tungsten needle, mounted in EMBED-812 epoxy, and ultra-microtomed. TEM analyses showed the olivines and orthopyroxenes to be equilibrated compared to those in anhydrous chondritic IDPs, and Fe-rich compared to hydrous chondritic IDPs. Furthermore, the olivines were Fe-rich compared to the ferromagnesian olivines from partially melted chondritic IDPs, which are typically on the order of Fo_{90} and En_{90}. Unlike common stratospheric particles, no magnesian-rich olivines or pyroxenes were found. In addition, shock processes had severely modified the few specimen investigated, as indicated by the presence of equilibrated, as well as shocked ferromagnesian minerals, recrystallization textures, glass, and melted metal and sulfide bodies decorating grain boundaries.

3.2 Orbital Debris

We established four subclasses of orbital debris: (1) Fe-Ni-Cr rich particles (Figure 2) representing stainless steel, (2) Zn-Ti-Cl rich residues representing thermal protective spacecraft paints, (3) Ag, Cu, or Pb-Sn rich residues originating from solar cell or other electrical and electronic components of spacecraft, and (4) pure aluminum impactors that were detectable only on the A03 gold surfaces; we do not know whether they were metallic or oxidized.

3.3 Indeterminate

Despite diligent efforts, a large number of craters did not yield spectra that contained measurable signals above that of the collector background. Efforts are underway to explore the utility of more sensitive analysis methods such as SIMS (Ref. 15) to attempt to characterize the impactor residues associated with such craters. However, it is known from laboratory impact experiments and modeling studies (Refs. 19, 20) that the projectile may be subjected to complete vaporization and/or ejected quantitatively as melt from the growing crater cavity during high-velocity impacts. Thus, the relative frequency of craters that contain insufficient residue for analysis by SEM/EDX methods may be a measure of the high-velocity component of both natural and man-made particle populations.

4. OBSERVED FREQUENCY

Figure 3 summarizes the analyses in histogram form, with the number of recognized projectile types plotted as a function of the associated crater size. The three major surfaces are plotted independently, as they represent different orientations (as well as materials). The intent is to illustrate the relative frequencies of the major particle types. As can be seen in Figure 3, the majority of events that contain *identifiable residues* were caused by natural, cosmic-dust particles, accounting for ~68% of the impactors on the A03 gold surfaces, ~77% on the A11 aluminum collectors, and 82% of those on the experiment-tray clamps. Other investigators (Refs. 15, 16, 17, 18) have analyzed projectile residues associated with LDEF craters from various surfaces, and their findings, although on fewer craters, are consistent with those illustrated in Figure 3.

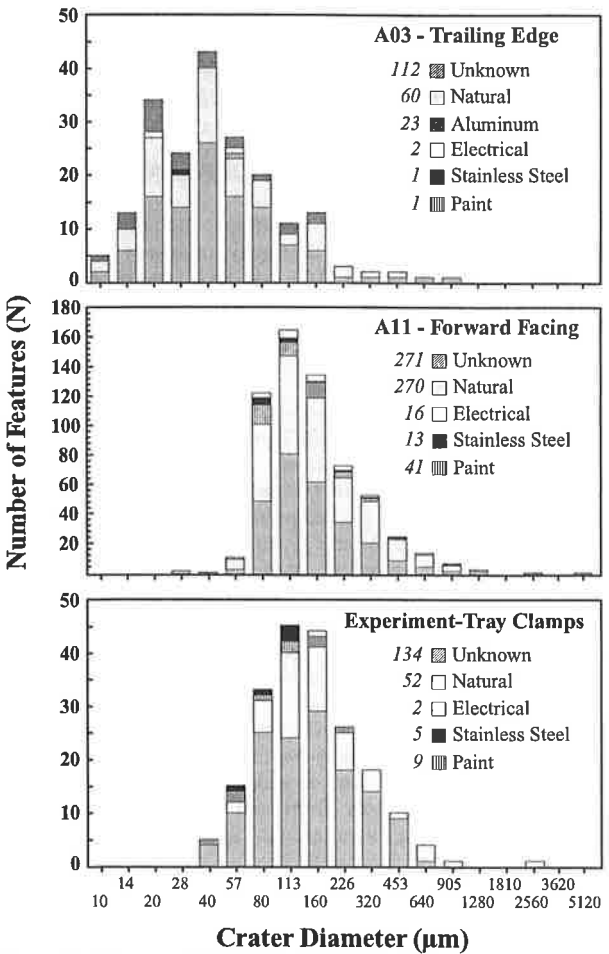

Figure 3. Histogram illustrating the relative distribution of the various particle types which impacted the CME surfaces (A03 and A11) and 44 experimental-tray clamps from Bay A.

Note the rather significant number of man-made debris particles which impacted the trailing edge of LDEF (*i.e.*, top histogram for A03). Prior to LDEF's return it was generally believed that there should be little or no interactions between LDEF's trailing edge and orbital debris. We find that man-made impactors constitute nearly 1/3 (27 of 87) of all *known* projectiles, and ~13% (27 of 199) of the entire crater population. The latter must be viewed as a minimum value. Data from the Interplanetary Dust Experiment (IDE; Refs. 8, 18) corroborate the unexpected result that a substantial flux of man-made debris must encounter the trailing edge of non-spinning platforms, such as LDEF or the planned Space Station *Freedom*. These findings necessitated a re-evaluation of the existing orbital-debris environment. Ref. 22 suggests that particles encountering LDEF's trailing edge should lie in highly elliptical orbits of low to medium inclination; such orbits are typical for transfer vehicles of payloads to geosynchronous orbit. These transfer vehicles are propelled by solid-fuel rocket motors, a well known source of aluminum particles in LEO (Refs. 17, 23). Furthermore, Ref. 22 suggests that the contribution to the total debris inventory from such transfer vehicles has been substantially underestimated.

In Figure 3 note that aluminum particles dominated the debris impactor for the trailing-edge gold surfaces; almost 90% (23 of 27) of the debris impacts were caused by aluminum, or ~12% (23 of 199) of the entire crater population. This seems to be consistent with aluminum from unburned fuels or of oxidized exhaust products.

If we combine all but the aluminum debris particles into a *miscellaneous* category, the latter occurs with a frequency of ~2% (4 of 199) on the trailing edge, ~12% (70 of 611) at the forward-facing A11 location, and ~8% (16 of 202) for the clamps; the clamps, presumably, represent an average value for the entire LDEF. Although the total number of *miscellaneous* impactors is small, resulting in poor statistics, especially for the trailing-edge surfaces, it appears that paint flakes are more numerous than the other materials.

5. PARTICLE-SIZE FREQUENCY

While Figure 3 correctly illustrates the observed, raw frequency data, it does not correctly represent the relative particle frequencies for the A03 and A11 viewing directions; the clamp data came from around the entire periphery of LDEF (Bay A) and will not be included in this discussion.

To facilitate the comparison between the two viewing directions we normalized the raw frequencies to a unit surface area (m^2) and exposure time (5.7 years; total LDEF mission). Furthermore, since the ultimate objective is to produce particle-size frequencies we utilized cratering mechanics and associated scaling laws to determine the size or mass of the impactors responsible for any given crater. The wide range in possible encounter velocities, angles of impact, and physical properties of the prospective projectiles (none of which is amenable to direct measurement during post-mortem investigation of individual craters) mandates a statistical approach that uses reasonable average conditions, as well as some assumptions. Conversion of crater size into projectile size is not without risk, and even more so if uncertainties in the velocity scaling (substantially beyond current laboratory data) of crater dimensions are considered. Nevertheless, we extracted projectile sizes from our present set of crater diameters using the assumptions and average conditions described below.

First, we assume a common density (*i.e.*, 2.7 g/cm^3) for all particles, which strictly applies to aluminum, but could also apply to a fair number of natural particles. We also assume a normal angle of incidence (*i.e.*, 90°) for all craters, a permissible assumption because the average velocities used in our conversions refer only to the normal velocity component. These assumptions are then combined with dynamic models predicting average encounter velocities for the forward-facing and trailing-edge viewing directions. For the A03 and A11 pointing directions we utilized velocities of ~12 and 23 km/s, respectively (Ref. 2), for natural particles. On the other hand, Ref. 22 modeled the orbital-debris environment and derived mean encounter velocities of ~2 and 8.3 km/s for the A03 and A11 sites, respectively.

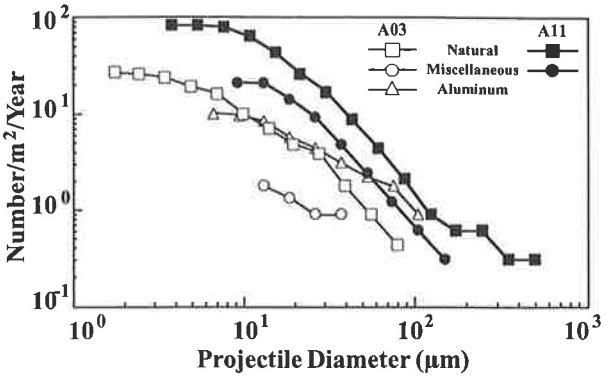

Figure 4. Particles fluxes for natural and man-made projectiles.

The resulting projectile-size frequencies and associated fluxes are illustrated in Figure 4. Note that we only calculated associated projectile diameter for craters of known origin. From these projectile-size frequencies we conclude: (a) The relative flux of natural impactors >10 μm in diameter differs by a factor of ~7 between the trailing and leading edges. (b) The number of miscellaneous impactors >20 μm in diameter appears to be ~10 times higher for the A11 location compared to LDEF's trailing edge. However, the absolute number of such impacts on the gold was only four, resulting in extremely poor statistics and large error bars associated with the trailing-edge flux for miscellaneous debris. (c) The size-frequency distribution of miscellaneous particles seems different for the A03 and A11 locations. The miscellaneous flux possesses a similar slope to that of the natural particles for the forward-facing direction, yet a noticeably shallower slope for the trailing-edge directions. (d) The largest impactors impinging upon the CME collectors appear to have been of natural cosmic-dust origins. Note that up to ~100 μm particles sizes, however, both natural and man-made are possible.

It should be noted that the observed crater and penetration features on LDEF *cannot* be interpreted properly by applying "global" average impact conditions (*e.g.*, Ref. 1 and many others) to any given set of impact features. The differences in the velocity regimes between natural and man-made particles are so substantial that they must be treated separately. At a minimum, LDEF investigators need a single, internally consistent, dynamic model that combines natural (*e.g.*, Ref. 2) and orbital-debris particles (*e.g.*, Ref. 22), and that estimates the absolute fluxes and mean velocities of these two populations such that appropriate weighting factors may be applied to any specific set of impact features for a non-spinning platform in LEO.

6. DISCUSSION

6.1 Loss Of Projectile Due To Vaporization

A large number of craters (~50%) did not yield analyzable projectile residues via the SEM-EDX techniques employed. We consider vaporization of the projectile during impact to be the major loss process, ultimately resulting in insufficient mass within the crater to yield significant X-ray counts. Because of the higher projectile velocities associated with the forward-facing A11 location, one would intuitively expect the higher shock-stresses and more vaporization on the forward-facing

surfaces which, however, is not observed. Therefore, we performed calculations to determine shock stresses and to explore the degree with which the density differences of the gold and aluminum targets may compensate for these velocity differences.

We utilized equation-of-state data for aluminum 6061, gold (Au), and anorthosite (An; a dense feldspar-rich rock, Ref. 25), and the thermodynamic model of Cintala (Ref. 26) that solves for the peak stress generated by aluminum and anorthosite impactors colliding with the CME collectors at velocities up to 25 km/s. In addition, Ref. 27's calculations that address the thermodynamic states and phase transitions of anorthosite upon pressure release were considered. Principally, all calculations employed two-dimensional shock geometries and apply specifically to the peak pressure at the target/projectile interface only, rather than to the bulk impactor.

For natural particles, that have encounter velocities of 12 and 23 km/s for the A03 and A11 locations, respectively, one obtains rather similar peak stresses for both collector materials. Therefore, it is not surprising to find a comparable number of craters which resisted SEM-EDX analysis for both CME orientations. This statement may be extended to particles of widely variable physical properties, such as low-density, high-porosity particles that should be common among interplanetary dust, unlike the (2.9 g/cm^3) anorthosite. As long as standard particles, even of widely variable physical properties, impact gold and aluminum at 12 and 23 km/s, respectively, grossly similar peak stresses will result. However, the absolute magnitude of stress depends strongly on the impactor itself, predominantly on its density. Absolute peak stress may be lower for low-density, porous dust particles, yet consider that low-density particles also require lower stresses for the onset of melting and vaporization (*e.g.*, Ref. 28).

Based on thermodynamic calculations (Ref. 27), substantial fractions of dense-silicate impactors are vaporized at conditions typical for LDEF encounters. From our computations, anorthosite particles impacting at velocities greater than ~14 and 25 km/s may be completely vaporized on gold and aluminum targets, respectively. Thus, the large fraction of indeterminate crater residues seems understandable.

As for orbital-debris particles, the low encounter velocities on the trailing edge result in peak pressures of ~50 GPa, which would not be high enough to vaporize most orbital-debris materials. However, because of the higher encounter velocities, peak stresses of ~100 GPa will be achieved on the forward-facing aluminum. Such pressures would be sufficient to melt a wide variety of materials, yet complete vaporization of the projectile should be rare.

However, overly specific conclusions are not warranted because each individual impact may have unique initial conditions. Our preferred inference is that the majority of indeterminate craters represent a velocity bias. This may not necessarily be the case, since a compositional bias, and the projectile's porosity may also apply (*e.g.*, volatile-rich impactors). Indeed, differences in the physical properties of the impactors result in significant differences in the onset of vaporization at otherwise identical initial conditions. Furthermore, it is possible that substantial fractions of impactor melts escaped the crater cavity at high-impact velocities (Ref. 20). Any of the above suggestions may combine to produce craters with little or no apparent residues.

One may safely conclude from our computations that most man-made impactors should result in analyzable residues for trailing-edge impacts, suggesting that all debris particles were accounted for on the gold collectors, and that all indeterminate craters on the trailing edge were the result of natural cosmic-dust impacts. Unfortunately, the situation for the forward-facing aluminum collectors is not as clear. The indeterminate fraction of craters at the A11 location must include all aluminum impactors, no matter what the encounter velocity, as well as a significant number of substantially vaporized cosmic-dust impacts, judging by their frequency on the trailing edge. The fraction of natural versus debris impacts responsible for the indeterminate residues on the aluminum surfaces remains basically unknown.

However, an attempt to estimate the number of aluminum impactors impinging upon the A11 location can be made using the data associated with the A03 location. Based on projectile-size considerations (Figure 4), the flux of aluminum projectiles at 20 μm in diameter is approximately a factor of four higher on the trailing edge than that of the *miscellaneous* debris. If one assumes that this relative frequency also applies to the A11 location, one could multiply the observed A11 miscellaneous-debris population at 20 μm (N=13/m^2/y; Figure 4) by a factor of four to obtain the prospective number of (non-analyzable) aluminum impactors for the A11 tray. This results in a total of ~54 aluminum particles >20 μm/m^2/y on the A11 surfaces. However, whether the distribution of aluminum to miscellaneous particles is similar for the geosynchronous transfer orbits as it is for the general LEO environment is not unknown.

6.2 Aluminum Particles On LDEF's Trailing Edge

The craters known to have resulted from orbital-debris particles that impacted the trailing-edge gold collectors did not possess the morphologies that would be expected from predominantly oblique (<45°), low-velocity (<2 km/s) impacts; such conditions should dominate for orbital-debris particle encountering the trailing edge (Ref. 22). Such conditions should lead to relatively shallow, substantially elongated, elliptical craters for orbital-debris particles (Refs. 29, 30), which should differ systematically from those associated with natural impactors. However, this was not observed on the A03 gold surfaces. Those craters in which man-made residues were detected did not differ morphologically from those that were caused by natural impactors. Certainly not in systematic fashion that would reflect the dominantly oblique, low-velocity trajectories of man-made particles. The observational (and experimental) database is presently insufficient to mandate revision of dynamic models, yet indications are that current observations and models appear at odds regarding the morphology of craters resulting from orbital-debris particle on LDEF's trailing edge.

As mention above, the most probable source for orbital-debris particles impinging upon LDEF's trailing edge is either unspent solid-fuel rocket fuel, or the exhaust by-products residing in the highly elliptical, low- to medium inclination geosynchronous transfer orbits (Ref. 22). In general, the exhaust by-products seem reasonable candidates for the smallest aluminum craters, yet not for those requiring projectiles >>10 μm in diameter (Ref. 23), which is necessary to produce ~40% of all aluminum events on the gold surfaces. The latter may be associated with unburned fuels left after premature shut-down of IUS motors, or failure to ignite in the first place. If this unburned fuel were exposed to space, differential erosion could readily produce free-flying metallic aluminum particles.

While we cannot be sure that this suggestion is valid, our point here is that the aluminum projectiles experienced by LDEF's trailing edge are not necessarily the result of collisionally or explosively fragmented structural components; solid-rocket fuels are a possible source of aluminum particles. Improved understanding of production mechanisms for orbital debris is needed to evaluate the relative roles of catastrophic comminution versus other processes so that improved

calculations of the number of parent satellites responsible for the current debris environment in high-eccentricity orbits are possible (Ref. 22). In addition, many paint flakes may not necessarily be derived from catastrophically destroyed satellites, but could be the spall products of numerous micro-impacts, even more so if radiation, thermal and atomic oxygen effects combine to render structurally weakened and degraded paint layers. The nature and potential role of mechanisms other than collisional and explosive fragmentation seem important in reconstructing the possible number of satellite parts involved (Ref. 22).

6. REFERENCES

1) Hörz, F., Bernhard, R.P., Warren, J., See, T.H., Brownlee, D.E., Laurance, M.R., Messenger, R., and Peterson, R.P., Preliminary Analysis of LDEF Instrument A0178-1 Chemistry of Micrometeoroids Experiment", *LDEF - 69 Months in Space, First Post-Retrieval Symposium, NASA CP-2434*, p. 487-501, 1991.

2) Zook, H. A., Deriving the Velocity Distribution of Meteoroids from The Measured Meteoroid Impact Directionality on the Various LDEF Surfaces, *LDEF - 69 Months in Space, First Post-Retrieval Symposium, NASA CP-2434*, p. 569-579, 1991.

3) Zolensky, M.E. ed., Particles from Collection Flag L2405, *Cosmic Dust Catalog, 11, 1, JSC # 24458-SN-83*, pp. 170, 1990.

4) Brownlee, D.E., Cosmic Dust: Collection and Research, *Ann. Rev. Earth. Planet. Sci., 13*, p.134-150, 1985.

5) Warren, J.L. and 10 co-authors, The Detection and Observation of Meteoroid and Space Debris Impact Features on the Solar Max Satellite, *Proc. Lunar Planet. Sci. Conf., 19th*, p. 641-657, 1989.

6) Bernhard, R.P. and McKay, D.S., Micrometer-Sized Impact Craters on Solar Maximum Satellite, *Lunar Planet. Sci. Conf., 19th*, p. 65-66, 1989.

7) Bernhard, R.P., *Impact Features on Returned Palapa Hardware*, Internal NASA Report, 1990.

8) Mullholland, J.D. and 8 co-authors, IDE Spatio-Temporal Fluxes and High Time-Resolution Studies of Multi-Impact Events and Long-Lived Debris Clouds, *LDEF - 69 Months in Space, First Post-Retrieval Symposium, NASA CP-3134*, p. 517-532, 1991.

9) McDonnell, J.A.M. and Sullivan, K., Dynamic (Computer) Modeling of the Particulate Environment: Transformations from the LDEF Reference Frame to Decode Geocentric and Interplanetary Populations, *LDEF - 69 Months in Space, First Post-Retrieval Symposium, NASA CP-3134*, p. 565-566, 1991.

10) Humes, D.H., Large Craters on the Meteoroid and Space Debris Impact Experiment, *LDEF - 69 Months in Space, First Post-Retrieval Symposium, NASA CP-3134*, p. 399-422, 1991.

11) See, T.H., Allbrooks, M., Atkinson, D., Simon, C. and Zolensky, M., *Meteoroid and Debris Impact Features Documented on the Long Duration Exposure Facility: A Preliminary Report*, NASA - Johnson Space Center Publication # 24608, pp. 583, 1990.

12) Crutcher, E.R., Nishimura, L.S., Warber, K.J., and Wascher, W.W., Migration and Generation of Contaminants from Launch Through Recovery: LDEF Case History, *LDEF - 69 Months in Space, First Post-Retrieval Symposium, NASA CP-3134*, p.125-140, 1991.

13) Schaal, R.B., Hörz, F., Thompson, T.D. and Bauer, J.F., Shock Metamorphism of Granulated Lunar Basalt, *Proc. Lunar Planet. Sci. Conf., 10th*, p. 2547-2571, 1979.

14) Stöffler, D., Deformation and Transformation of Rock-Forming Minerals by Natural and Experimental Shock Processes; Behavior of Minerals under Shock Compression, *Fortschr. Mineral., 49*, p. 50-113, 1972.

15) Amari, S., Foote, J., Simon, C., Swan, P., Walker, R.M. , Zinner, E., Jessberger, E.K., Lange, G. and Stadermann, F., SIMS Chemical Analysis of Extended Impact Features from the Trailing Edge Portion of Experiment A0191-2, *LDEF - 69 Months in Space, First Post-Retrieval Symposium, NASA CP-3134*, p. 503-516, 1991.

16) Mandeville, J.C. and Borg, J., Study of Dust Particles On-Board LDEF: The FRECOPA Experiments A0138-1 and A0138-2, *LDEF 69 Months in Space, First Post -Retrieval Symposium, NASA CP-3134*, p. 419-434, 1991.

17) Amari, S., Foote, J. Swan, P., Walker, R.M., Zinner, E., and Lange, G., SIMS Chemical Analysis of Extended Impacts in the Leading and Trailing Edges of LDEF Experiment A0231-2, *LDEF - 69 Months in Space, Second Post-Retrieval Symposium, NASA CP-1394, in press*, 1993.

18) Simon, C.G., Hunter, J.L., Griffis, D.P., Misra, V., Ricks, D.A., Wortmann, J.J., and Brownlee, D.E., Elemental Analyses of Hypervelocity Microparticle Impact Sites on Interplanetary Dust Experiment Sensor Surfaces, *LDEF - 69 Months in Space, Second Post-Retrieval Symposium, NASA CP-1394, in press*, 1993.

19) Bernhard, R.P, See, T.H., and Hörz, F., Projectile Compositions And Modal Frequencies On The "Chemistry Of Micrometeoroids" LDEF Experiment. *LDEF - 69 Months in Space, Second Post-Retrieval Symposium, NASA CP-1394, in press*, 1993.

20) Coombs, C., Watts, A., Wagner, J., and Atkinson, D., LDEF Data: Comparison with Existing Models, *LDEF - 69 Months in Space, Second Post-Retrieval Symposium, NASA CP-1394, in press*, 1993.

21) Kessler, D.J., Reynolds, R.C. and Anz-Meador, P.D., *Orbital Debris Environment for Spacecraft Designed to Operate in Low Earth Orbit, NASA TM-100-471*, 1988.

22) Kessler, D. J., Origin of Orbital Debris Impacts on Long Duration Exposure Facility's (LDEF) Trailing Surfaces (abstract), *Second LDEF Post-Retrieval Symposium Abstracts*, p. 53, 1992.

23) VerPloeg, K.L. and McKay, D.S., Impacts on Shuttle Orbiter Caused by the Firing of a PAM D2 Solid Rocket: Results of the STS-58B Plume Witness Plate Experiment. NASA Report on Orbital Debris, 1989.

24) Cour-Palais, B.G., Hypervelocity Impacts into Metals, Glass, and Composites, *Int. J. Imp. Eng., 5*, p. 225-237, 1987.

25) Marsh, S.P., ed., LASL Shock Hugoniot Data, University of California Press, pp. 658, 1980.

26) Cintala, M. J., Impact-Induced Thermal Effects in the Lunar and Mercurian Regoliths, *J. Geophys. Res., 97*, p. 947-973, 1992.

27) Ahrens, T.J. and O'Keefe, J.D., Equations of State and Impact-Induced Shock Wave Attenuation on the Moon, in *Impact and Explosion Cratering*, Roddy *et al.*, eds., Pergamon Press, New York, p. 639-656, 1976.

28) Kieffer, S.W., Shock Metamorphism of the Coconino Sandstone at Meteor Crater, Arizona, *J. Geophys. Res., 76*, p. 5449-5473, 1971.

29) Gault, D. E., Displaced Mass, Depth, Diameter and Effects of Oblique Trajectories for Impact Craters Formed in Dense Crystalline Rock , *The Moon , 6*, p. 25-44, 1973.

30) Herrmann, W. and Wilbeck, J.S., Review of Hypervelocity Penetration Theories, *Int. J. Impact Engn, 5*. p. 237-252, 1987.